Distinct nonequilibrium plasma chemistry of C_2 affecting the synthesis of nanodiamond thin films from C_2H_2 (1%)/H_2/Ar-rich plasmas

F. J. Gordillo-Vázquez[a)]
Instituto de Óptica, C.S.I.C., Serrano 121, 28006 Madrid, Spain

J. M. Albella
Instituto de Materiales de Madrid, C.S.I.C., Cantoblanco, 28049 Madrid, Spain

(Received 29 May 2003; accepted 15 August 2003)

We show that the concentrations of the species $C_2(X\,^1\Sigma_g^+)$, $C_2(a\,^3\Pi_u)$, and C_2H exhibit a significant increase when the argon content grows up to 95% in medium pressure (0.75 Torr) radio frequency (rf) (13.56 MHz) produced C_2H_2 (1%)/H_2/Ar plasmas of interest for the synthesis of nanodiamond thin films within plasma enhanced chemical vapor deposition devices. In contrast, the concentrations of CH_3 and C_2H_2 remain practically constant. The latter results have been obtained with an improved quasianalytic space–time-averaged kinetic model that, in addition, has allowed us to identify and quantify the relative importance of the different underlying mechanisms driving the nonequilibrium plasma chemistry of C_2. The results presented here are in agreement with recent experimental results from rf CH_4/H_2/Ar-rich plasmas and suggest that the growth of nanodiamond thin films from hydrocarbon/Ar-rich plasmas is very sensitive to the contribution of C_2 and C_2H species from the plasma. © *2003 American Institute of Physics.* [DOI: 10.1063/1.1617362]

I. INTRODUCTION

Experimental results on the synthesis of nanocrystalline diamond thin films in a matrix of diamond like carbon by Amaratunga *et al.*[1] working with radio-frequency (rf) (13.56 MHz) produced CH_4 (2%)/Ar plasmas at medium pressures (0.3–0.5 Torr), together with the most recent results by Gruen and co-workers[2–10] with microwave (MW) (2.45 GHz) excited CH_4 (1%)/H_2/Ar plasmas at high pressures (50–100 Torr), have shown the feasibility of growing nanocrystalline diamond thin films by using plasma mixtures of different carbon containing molecules (CH_4,C_{60}) with minute amounts of molecular hydrogen (from 0% to 1%) and important argon concentrations (up to 99%). In addition, the systematic experiments carried out by Zhou *et al.*[7] show a transition from microdiamond to nanodiamond with the presence, in the latter case, of strong Swan band emission related to C_2 radicals. The micro- to nanodiamond transition has been shown to be especially sensitive to the amount of Ar in the plasma since optical emission spectroscopy experiments in the plasma show dramatic changes in the species emission pattern as the Ar concentration increases.[6,7,10] This suggests that changes in the nonequilibrium plasma chemistry are likely to occur parallel to the surface changes leading from micro- to nanodiamond structures.

While some experimental evidence points to C_2 dimers as the growth species for nanocrystalline diamond in MW CH_4 (1%)/H_2/Ar and C_{60}/Ar plasmas, a lack of understanding remains with regard to the different reaction paths that lead to the increase of the C_2 species when Ar increases. In addition, dicarbon (C_2) radicals together with C_2H species (not studied experimentally as a function of Ar) might also be responsible for the diamond nanocrystals found in rf medium pressure CH_4 (2%)/Ar plasmas[1] since C_2H exhibit higher chemisorption probabilities than CH_3, CH_4, and C_2H_2.[11]

Therefore, the main goal of this article is to discuss the nonequilibrium plasma chemistry of the C_2 and $C_2(a\,^3\Pi_u)$ (hereafter, called C_2*) species produced in rf (13.56 MHz)-generated C_2H_2 (1%)/H_2/Ar at medium pressure (0.75 Torr) plasmas of interest in nanodiamond thin film deposition. This will be done in connection with the predicted trend of other important species such as C_2H, CH_3, and C_2H_2. We propose a number of kinetic mechanisms that account for the experimental trend of the radical CH_3 observed by Schulz-von der Gathen *et al.*[12] in rf (13.56 MHz)-generated hydrocarbon/Ar-rich plasma environments.

Finally, we will also compare our model results with recent simulations by Riccardi *et al.*[13] of the gas-phase chemistry of rf, medium pressure ($0.75\,\text{Torr} \leqslant p \leqslant 1.5\,\text{Torr}$) CH_4/Ar plasmas. The latter results are interesting since they indicate that CH_3 is the most abundant carbon-containing radical in pure rf CH_4 discharges, while it is the dimer C_2 in discharges of CH_4 highly diluted in argon. However, the latter simulations fail to predict the experimentally observed trends for the concentrations of the radical CH_3. Moreover, our own previous results[14] (using a very simplified C_2 chemistry) together with Riccardi's simulations[13] predicted unrealistically high values ($\sim 10^{13}\,\text{cm}^{-3}$ for 90% of Ar in the feed gas) for the concentration of C_2. The latter concentrations have not even been measured within the high pressure (50–100 Torr) and power (1000 W) MW (2.45 GHz)-produced CH_4/H_2/Ar-rich plasmas studied by Gruen and co-workers.[2–10] In the present work, the different chemical reaction paths assumed for the C_2 species allow us to

[a)]Author to whom correspondence should be addressed; electronic mail: vazquez@io.cfmac.csic.es

TABLE I. Electron-impact processes.

Reaction	Reaction
$e+Ar \rightarrow e+Ar^*(n=2,{}^1P_1,{}^3P_{0,1,2})$	$H^*(n=2,{}^2P^0{}_{1/2,3/2})+e \rightarrow e+H$
$e+Ar \rightarrow 2e+Ar^+$	$e+C_2H_2 \rightarrow 2e+C_2H_2{}^+$
$e+Ar^*(n=2,{}^3P_{0,2}) \rightarrow e+Ar$	$e+C_2H_2 \rightarrow C_2H+2H+e$
$e+e+Ar^+ \rightarrow e+Ar$	$e+C_2 \rightarrow C_2{}^*+e$
$e+Ar^+ \rightarrow Ar+h\nu$	$e+C_2H_2{}^+ \rightarrow C_2+H+H$
$e+H_2 \rightarrow H+H+e$	$e+C_2H_2{}^+ \rightarrow C_2{}^*+H+H$
$e+H_2 \rightarrow 2H^*(n=2,{}^2P^0{}_{1/2,3/2})+e$	$e+C_2H_2{}^+ \rightarrow C_2H+H$
$e+H_2 \rightarrow H+H^{**}(n=3,{}^2P^0{}_{1/2,3/2})+e$	$e+C_2H \rightarrow C+C+H+e$
$e+H_2 \rightarrow H_2{}^++2e$	$e+CH_4 \rightarrow CH_3+H+e$
$e+H_2 \rightarrow e$	$e+C_2H_3 \rightarrow C_2H+2H+e$
$+H_2{}^*(B\,{}^1\Sigma^+{}_u, C\,{}^1\Pi_u, a\,{}^3\Sigma^+{}_g)$	
$e+H_2 \rightarrow e+H_2{}^*(b\,{}^3\Sigma^+{}_u, c\,{}^3\Pi_u, d\,{}^3\Pi_u)$	$e+C_2H_3 \rightarrow C_2H_2+H+e$
$e+H_2(v=0) \rightarrow e+H_2(v=1,2,3)$	$e+C_2H_2{}^+ \rightarrow CH+CH$
$e+H \rightarrow e+H^*(n=2,{}^2P^0{}_{1/2,3/2})$	$e+C_2H_2{}^+ \rightarrow CH_2{}^*+C$

predict concentrations for C_2 and $C_2{}^*$ that are reasonable for the pressure conditions studied (see below) that, in addition, keep the experimentally observed trends (in MW plasmas) with increasing Ar content in the feed gas.

II. APPROACH

We have used a general quasianalytic space–time-averaged (zero-dimensional) kinetic model for studying the nonequilibrium plasma chemistry of medium-pressure (0.75 Torr) C_2H_2 (1%)/H_2/Ar rf plasmas ($f=13.56$ MHz, $\phi_{\text{Total}}=100$ sccm, $P=100$ W) with a gas temperature of $T_g=400$ K.[14] The latter simulation conditions were chosen so as to compare with the recent diagnosis studies reported by Schulz-von der Gathen *et al.*[12] for capacitively coupled rf (13.56 MHz) plasmas containing $CH_4/H_2/Ar$.

The model that we have used here is based on a previous one.[14] The differences are, however, that we have now considered more types of species [Ar,$Ar^*(n=2,{}^1P_1,{}^3P_{0,1,2})$, Ar^+, $ArH^*(B\,{}^2\Pi, E\,{}^2\Pi, 1\,{}^2\Delta)$, H_2, $H_2{}^*$ ($B\,{}^1\Sigma^+{}_u$, $C\,{}^1\Pi_u$, $a\,{}^3\Sigma^+{}_g$, $b\,{}^3\Sigma^+{}_u$, $c\,{}^3\Pi_u$, $d\,{}^3\Pi_u$), H, $H^*(n=2,{}^2P^0{}_{1/2,3/2})$, CH, CH_2, CH_3, CH_4, C_2H_2, $C_2H_2{}^+$, C_2H_3, C_2H, C_2, $C_2{}^*$] together with a greater number of possible reaction paths for each of the species considered, including electron-impact processes (Table I),[14–16] radiative processes (Table II),[14,17] and neutral–neutral and neutral–ion mechanisms [see Table III (Refs. 18–23) and Table IV (Refs. 20, 21, 24, and 25)]. It is worth mentioning that the dissociation reactions of the type CH_2+Ar and CH+Ar (Ref. 23) are not included in the model equations since their important barrier heights avoid them to proceed in low gas temperature (and medium pressure) environments like ours. However, the reactions $CH_2/CH+Ar$ could probably proceed in the dissociation direction in the case of the high pressure and high power MW-generated $CH_4/H_2/Ar$-rich plasmas studied by Gruen and co-workers.[2–10] In these plasmas, the measured gas temperatures take values of up to 1500 K, that is, close to the gas temperature region where the rate coefficients of the reactions $CH_2/CH+Ar$ have been experimentally evaluated.[23]

The present model provides a period-average electron energy distribution function (EEDF) that is obtained from the numerical solution of an electron Boltzmann equation solved under the assumption of a two-term approach based on the dc effective field approximation which, as shown in a previous work,[14] is justified for the case of rf (13.56 MHz) produced C_2H_2 (1%)/H_2/Ar plasmas. Once the period average

TABLE II. Radiative processes and their corresponding rate coefficients.

Reaction	Rate coefficient (s^{-1})
$Ar^*(n=2,{}^1P_1,{}^3P_1) \rightarrow Ar+h\nu$	3.00×10^8
$ArH^*(B\,{}^2\Pi, E\,{}^2\Pi, 1^2\Delta) \rightarrow Ar+H+h\nu$	5.93×10^7, 2.85×10^7, 3.40×10^7
$H^*(n=2,{}^2P^0{}_{1/2,3/2}) \rightarrow H+h\nu$	4.70×10^7

TABLE III. Neutral–neutral and neutral–ion processes and their corresponding rate coefficients.

Reaction	Rate coefficient ($cm^3\,s^{-1}$ or $cm^6\,s^{-1}$)
$Ar^*(n=2,{}^3P_{0,2})+C_2H_2 \rightarrow C_2H_2{}^++Ar+e$	3.50×10^{-10}
$Ar^++C_2H_2 \rightarrow C_2H_2{}^++Ar$	4.20×10^{-10}
$Ar^*(n=2,{}^3P_{0,2})+H_2 \rightarrow ArH^*+H$	1.10×10^{-10}
$Ar^++H_2 \rightarrow H_2{}^++Ar$	3.00×10^{-9}
$Ar^++H_2 \rightarrow ArH^++H$	5.40×10^{-10}
$CH+CH \rightarrow C_2H+H$	2.49×10^{-10}
$Ar+C_2H_2+H \rightarrow C_2H+H_2+Ar$	8.79×10^{-31}
$C_2H+H \rightarrow C_2H_2$	3.00×10^{-10}
$Ar+C_2H+H \rightarrow C_2H_2+Ar$	3.10×10^{-32}
$C_2H+H_2 \rightarrow C_2H_2+H$	1.51×10^{-13}
$CH_3+H \rightarrow CH_4$	7.00×10^{-12}
$CH_3+C_2H_2 \rightarrow CH_4+C_2H$	7.63×10^{-26}
$CH_3+H_2 \rightarrow CH_4+H$	1.16×10^{-20}
$CH_3+H+Ar \rightarrow CH_4+Ar$	8.19×10^{-29}
$CH_4+CH \rightarrow C_2H_4+H$	6.42×10^{-11}
$CH_3+CH \rightarrow C_2H_3+H$	4.98×10^{-11}
$CH_2+CH_2 \rightarrow C_2H_3+H$	3.32×10^{-11}
$C_2H_2+H \rightarrow C_2H_3$	1.60×10^{-13}
$C_2H_3+Ar \rightarrow C_2H_2+H+Ar$	1.30×10^{-12}
$C_2H_3 \rightarrow C_2H_2+H$	3.31×10^{-14}

TABLE IV. Neutral–neutral processes and their corresponding rate coefficients.

Reaction	Rate coefficient ($cm^3\,s^{-1}$)
$C_2H_3+H \rightarrow C_2H_2+H_2$	1.60×10^{-12}
$C_2H_3+H \rightarrow C_2H_4$	4.80×10^{-11}
$C_2H_3+H_2 \rightarrow C_2H_4+H$	9.81×10^{-20}
$CH_2+CH_2 \rightarrow CH_3+CH$	7.68×10^{-13}
$CH_2+H_2 \rightarrow CH_3+H$	5.00×10^{-15}
$C_2H_3+CH_2 \rightarrow C_2H_2+CH_3$	3.00×10^{-11}
$CH_3+CH_3 \rightarrow C_2H_6$	4.36×10^{-11}
$CH(X\,{}^2\Pi, v=1)+H_2 \rightarrow CH_3$	1.60×10^{-10}
$CH_3+Ar^*(n=2,{}^3P_{0,2}) \rightarrow CH_3{}^{+*}+Ar+e$	2.60×10^{-10}
$CH_3+CH_2 \rightarrow C_2H_4+H$	7.00×10^{-11}
$CH_3+C_2H_3 \rightarrow CH_4+C_2H_2$	6.50×10^{-13}
$CH_2+Ar^*(n=2,{}^3P_{0,2}) \rightarrow CH_2{}^{+*}+Ar+e$	2.60×10^{-10}
$CH_2+Ar^*(n=2,{}^3P_{0,2}) \rightarrow C+H_2+Ar$	5.00×10^{-10}
$CH_2+H \rightarrow CH+H_2$	2.70×10^{-10}
$CH+H_2 \rightarrow CH_2+H$	3.03×10^{-11}
$CH+Ar^*(n=2,{}^3P_{0,2}) \rightarrow C+H+Ar$	5.00×10^{-10}
$CH+Ar^*(n=2,{}^3P_{0,2}) \rightarrow CH^{+*}+Ar+e$	2.60×10^{-10}
$CH+H \rightarrow C+H_2$	4.98×10^{-11}

TABLE V. Electron-impact and neutral–neutral reaction paths controlling the behavior of C_2 and C_2*, and their corresponding rate coefficients.

Reaction	Rate coefficient ($cm^3\,s^{-1}$)
$C_2H+C_2H \rightarrow C_2+C_2H_2$	3.0×10^{-12} (k_1)
$C_2H+H \rightarrow C_2+H_2$	1.54×10^{-31} (k_2)
$C_2H_2+Ar \rightarrow C_2+H_2+Ar$	5.71×10^{-18} (k_3)
$e+C_2 \rightarrow e+C_2^*(a\,^3\Pi_u)$	$\cong 2.0\times10^{-8}$ (k_4)
$C_2+H_2 \rightarrow C_2H+H$	1.40×10^{-12} (k_5)
$C_2^*(a\,^3\Pi_u)+C_2H_2 \rightarrow 2C_2H^*$	9.6×10^{-11} (k_6)
$C_2^*(a\,^3\Pi_u)+H_2 \rightarrow C_2H+H$	$<9.0\times10^{-14}$ (k_7)
$C_2+Ar^*(n=2,{}^3P_{0,2}) \rightarrow C_2^{+}+e+Ar$	5.6×10^{-10} (k_8)
$e+C_2H_2^{+} \rightarrow C_2^*(a\,^3\Pi_u)+H+H$	1.3×10^{-8} (2.5 eV) -0.86×10^{-8} (5.6 eV) (k_9)

EEDF is available, we can derive the corresponding period average electron-impact rate coefficients that are used later on in a set of kinetic rate equations accounting for the non-equilibrium chemistry of C_2H_2 (1%)/H_2/Ar plasmas. Due to the limitations of the Boltzmann solver used[26] (restricted to three species), the calculations of electron-rate coefficients involving the use of a non-Maxwellian EEDF are carried out for species C_2H_2, H_2, and Ar.

The model used here allows us to derive approximate analytical expressions that help us to discover interesting features related to the microscopic reaction paths underlying the variation of the different particle population densities considered. We have assumed that at 0.75 Torr the value of the electron density is $N_e=3.4\times10^{10}\,cm^{-3}$ and that, according to experimental results,[12] it remains practically constant with the variation of the Ar concentration in the plasma. Additional details of the approach can be found in Ref. 14.

In the following, we will focus on the reaction paths underlying the concentrations of C_2 and C_2* (see Table V), which exhibit an important increase when the amount of Ar in the plasma grows.

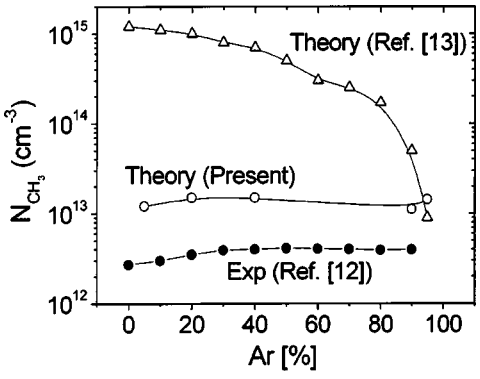

FIG. 1. Steady state concentrations of CH_3 as a function of the Ar content in the feed gas according to the present model (○) [rf (13.56 MHz) C_2H_2 (1%)/H_2/Ar plasma, $p=0.75$ Torr, power=100 W, and $\phi_{Total}=100$ sccm], the simulation results by Riccardi *et al.* (Ref. 13) (△) (rf CH_4/Ar plasma with $p=1.5$ Torr, power=50 W, and $\phi_{Total}=120$ sccm), and according to the experimental results by Schulz-von der Gathen *et al.* (Ref. 12) (●) [rf (13.56 MHz) CH_4 (10%)/H_2/Ar plasma with p=0.75 Torr, power=100 W, and $\phi_{Total}=66$ sccm]. The solid lines are a guide for the eye.

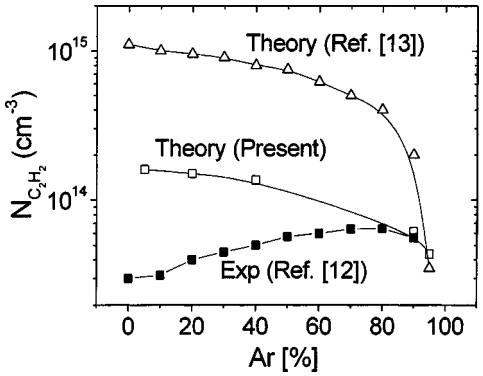

FIG. 2. Steady state concentrations of C_2H_2 as a function of the Ar content in the feed gas according to the present model (□) [rf (13.56 MHz) C_2H_2 (1%)/H_2/Ar plasma, $p=0.75$ Torr, power=100 W, and $\phi_{Total}=100$ sccm], the simulation results by Riccardi *et al.* (Ref. 13) (△) (rf CH_4/Ar plasma with $p=1.5$ Torr, power=50 W, and $\phi_{Total}=120$ sccm), and according to the experimental results by Schulz-von der Gathen *et al.* (Ref. 12) (■) [rf (13.56 MHz) CH_4 (10%)/H_2/Ar plasma with $p=0.75$ Torr, power=100 W, and $\phi_{Total}=66$ sccm]. The solid lines are a guide for the eye.

III. RESULTS AND DISCUSSION

We see in Figs. 1 and 2 that the concentrations of CH_3 and C_2H_2 predicted by the model follow, in a quite reasonable way, the experimental concentrations obtained by Schulz-von der Gathen *et al.*[12] for medium pressure (0.75 Torr) capacitively coupled rf (13.56 MHz) plasmas containing $CH_4/H_2/Ar$. In the latter rf plasmas, the degree of dissociation of CH_4 leading to C_2H_2 is quite high for low ($\leqslant$10%) methane concentrations,[12,27] and it increases as the Ar content grows.[12] Therefore, we can simulate the $CH_4/H_2/Ar$ plasma as it was one of $C_2H_2/H_2/Ar$ so that our results can be compared to the experimental results reported by Schulz-von der Gathen *et al.*[12] It is interesting to note that, according to Figs. 1 and 2, using high Ar concentration hardly affects the experimental and theoretical concentrations of CH_3 and C_2H_2. In other words, the latter results suggest that the species CH_3 and C_2H_2 are not particularly sensitive to an important increase of the Ar amount in the plasma. However, in contrast to this, there are experimental results indicating that the synthesis of nanodiamond thin films from medium pressure (0.2–0.5 Torr) rf (13.56 MHz) CH_4/Ar (Ref. 1) and high pressure (50–100 Torr) MW (2.45 GHz) $CH_4/H_2/Ar$ plasmas[2–8,10] is only possible when the Ar content increases up to sufficiently high values (usually, 80%–99%). Therefore, the above results suggest that the role played by C_2H_2 and the radical CH_3 during the growth of nanodiamond films might not be very important. In this regard, it is important to note that previous simulations of rf CH_4/Ar-rich plasmas by Riccardi *et al.*[13] fail to predict the experimental trends (and quantitative values) of the CH_3 and C_2H_2 densities recently measured by Schulz-von der Gathen *et al.*[12]

When we look at Fig. 3, we can see that our kinetic model predicts that, as the Ar content increases, the concentrations of C_2 (also predicted by Riccardi *et al.*[13]) and C_2*, and of C_2H exhibit significant growth. The increase of C_2* with growing Ar concentration has been experimentally observed (at a fixed pressure of 100 Torr) by Gruen and coworkers during their works with high pressure (50–100 Torr)

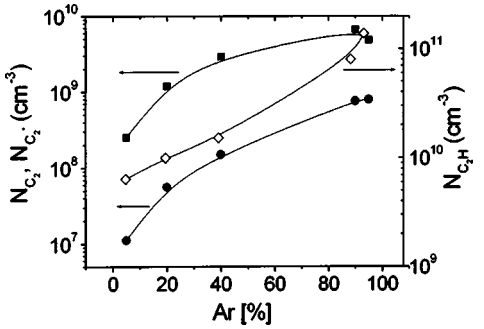

FIG. 3. Steady state concentrations of C_2 (■), C_2* (●), and C_2H (◇) as a function of the Ar content in the feed gas according to the present model for a rf (13.56 MHz)-produced C_2H_2 (1%)/H_2/Ar plasma at 0.75 Torr and 100 W with $\phi_{Total}=100$ sccm. The solid lines are a guide for the eye.

MW (2.45 GHz)-produced $CH_4/H_2/Ar$ plasmas.[2–10] Moreover, the deposits of nanodiamond thin films coincide with the observation of intense emission lines belonging to the different vibrational transitions within the Swan band of C_2.[5–7,10] The latter experimental results suggest the existence of different reaction paths driving the nonequilibrium plasma chemistry that leads to the changes observed in the C_2* emission pattern as the Ar content in the plasma increases.

Contrary to the optical diagnosis studies of C_2* carried out (as a function of the Ar concentration) in the $CH_4/H_2/Ar$ plasmas produced by MW,[10] there is a lack of similar experimental results within medium pressure rf (13.56 MHz) $CH_4/H_2/Ar$ plasmas and/or other hydrocarbon/Ar-rich plasma environments. Therefore, at the present stage, the results of Fig. 3 can only be compared with those obtained in high pressure (50–100 Torr) MW $CH_4/H_2/Ar$ plasmas with which a qualitative agreement is obtained.[6]

In order to discuss the different kinetic processes (shown in Table V) underlying the loss of C_2 and C_2*, we use two approximate analytic equations from our kinetic model. Thus, the concentrations of C_2 and C_2* shown in Fig. 3 are given by the equations:

$$N_{C_2}=\frac{N_{C_2H}(N_{C_2H}k_1+N_Hk_2)+N_{c_2H_2}N_{Ar}k_3}{N_ek_4+N_{H_2}k_5}, \quad (1)$$

and

$$N_{C_2^*}=\frac{N_eN_{C_2}k_4}{N_{C_2H_2}k_6}, \quad (2)$$

where k_1-k_6 are rate coefficients given in Table V. The loss of C_2* through reactions of the type $C_2^*+H_2$ with reaction rate k_7 (Ref. 28) are, in general, negligible and, therefore, not considered in expression (2). In addition, although Penning ionization (with rate k_8) of C_2 by metastable Ar atoms is possible,[29] this process is not important when compared to the loss of C_2 through mechanisms (4) and (5) of Table V.[28] The rate k_4 for the electron-impact excitation of C_2 remains practically constant within the interval of average electron energies obtained in the present work (see Table VI and Ref. 16).

TABLE VI. Average electron energies $\langle\epsilon\rangle$ obtained from the kinetic model of the rf (13.56 MHz)-produced C_2H_2 (1%)/H_2/Ar plasma at 0.75 Torr, $T_g=400$ K, and 100 W for the different considered Ar contents in the feed gas.

Ar (%)	$\langle\epsilon\rangle$
5	2.52
20	2.91
40	3.48
90	5.26
95	5.59

Experimental branching ratios regarding the electronic dissociative recombination of the $C_2H_2^+$ molecular ion have been recently measured by Derkatch *et al.*[30] They found that the electron dissociative recombination of $C_2H_2^+$ is dominated by the two-body C_2H+H channel followed by the three-body C_2+H+H, with branching ratios of 0.50 ± 0.06 and 0.30 ± 0.05, respectively, for very low energy electrons (between 0 and 0.0074 eV).

In a preliminar approximation we have not considered the second channel leading to C_2+H+H since we have considered that the main contribution of the electronic dissociative recombination of $C_2H_2^+$ is to produce C_2H radicals. In addition, it is not clear whether the above branching ratios remain valid for the much higher electron energies obtained in our calculations (ranging from 2.52 eV for 5% Ar to 5.59 eV for 95% Ar at the fixed pressure of 0.75 Torr, see Table VI). Moreover, as suggested by Derkatch *et al.*,[30] if more electronic energy is available a broader range of vibrational levels in C_2 would be accessible. Eventually, for high enough electron energies, this channel would have access to the lowest excited electronic level of C_2, that is, $C_2(a\,^3\Pi_u)=C_2$*, which is just 0.088 eV above the ground electronic state of C_2. Consequently, we then should consider not $e+C_2H_2^+\rightarrow C_2+H+H$, but $e+C_2H_2^+\rightarrow C_2^*+H+H$. In the latter case, the production of C_2* would not change much if we accept as a valid rate coefficient the one reported by Fantz *et al.*[16] for the electronic excitation of C_2 (see k_4 in Table V).

Therefore, if we consider the branching ratios reported by Derkatch *et al.*[30] and the cross section for the electronic dissociative recombination of $C_2H_2^+$ provided by Brooks *et al.*,[15] we find that, for the energies of our plasma and considering a Maxwellian EEDF, the rate coefficient for electronic dissociative recombination of $C_2H_2^+$ would go from $k_9=1.3\times10^{-8}\,cm^3\,s^{-1}$ (for 2.52 eV) to $k_9=0.86\times10^{-8}\,cm^3\,s^{-1}$ (for 5.59 eV), which are smaller than the considered rate coefficients [$\sim2.1\times10^{-8}\,cm^3\,s^{-1}$ (2.5 eV) and $\sim3.5\times10^{-8}\,cm^3\,s^{-1}$ (6.0 eV), being both derived using a Maxwellian EEDF] reported by Fantz *et al.*[16] for the production of C_2* from the electron-impact excitation of C_2. Consequently, the use of channel $e+C_2H_2^+\rightarrow C_2+H+H$ might most probably turn into $e+C_2H_2^+\rightarrow C_2^*+H+H$ for high enough electron energies as the ones of our plasma, and its impact on the production of C_2* might be moderate (less than factor 2) for the case of 5% Ar and very small for 95% Ar.

The concentrations for C_2H_2 and C_2H predicted by the

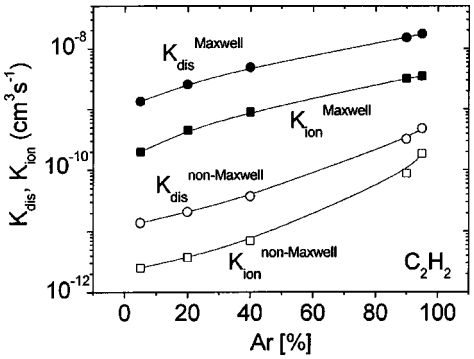

FIG. 4. Electron impact ionization (■ and □ for a Maxwellian and a non-Maxwellian EEDF, respectively) and dissociation (● and ○ for a Maxwellian and a non-Maxwellian EEDF, respectively) of C_2H_2 as a function of the Ar content in the feed gas according to the present model for a rf (13.56 MHz)-produced C_2H_2 (1%)/H_2/Ar plasma at 0.75 Torr and 100 W with $\phi_{Total}=100$ sccm. The solid lines are a guide for the eye.

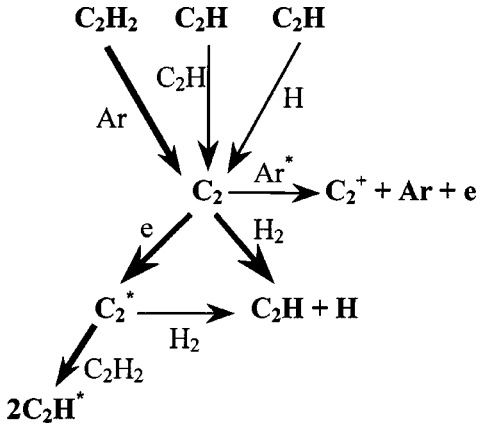

FIG. 5. Schematic representation of the different reaction paths underlying the values of the concentrations of C_2 and C_2* predicted in the present work for a rf (13.56 MHz) C_2H_2 (1%)/H_2/Ar plasma at 0.75 Torr and 100 W with $\phi_{Total}=100$ sccm. The thicker lines indicate the dominant reaction mechanisms.

model can be seen in, respectively, Figs. 2 and 3. The densities corresponding to H, H_2, and Ar are not shown but their trends are such that (as expected), whereas N_H and N_{H_2} decrease, N_{Ar} grows with increasing Ar content in the plasma.

According to our model, the production of C_2 is controlled, within the entire Ar range, by the dissociation of C_2H_2 due to collisions with Ar atoms. In fact, the latter mechanism accounts for more than the 99% of the C_2 production channels. It is worth mentioning that, although the collision of two C_2H molecules is, in principle, favored (over the C_2H_2+Ar mechanism) by a greater rate coefficient ($3\times10^{-12}\,cm^3\,s^{-1}$), the higher concentrations of C_2H_2, and especially of Ar, with respect to that of C_2H (approximately six orders of magnitude lower than the one of Ar), makes of the dissociation of C_2H_2 with Ar atoms the dominant reaction pathway leading to C_2. However, the importance of the reaction $C_2H_2+Ar\rightarrow C_2+H_2+Ar$ as a loss mechanism of C_2H_2 is negligible when compared to other C_2H_2 loss processes with much higher (about eight orders of magnitude) rate coefficients like, for instance, Penning ionization with resonant and/or metastable Ar atoms [$C_2H_2+Ar(^1P_1,{}^3P_{0,1,2})\rightarrow {C_2H_2}^+ + Ar + e$] and electron-impact mechanisms such as C_2H_2 ionization and dissociation ($e+C_2H_2\rightarrow C_2H+H+e$). In all the latter processes, their important rate coefficients compensate the smaller concentrations (with respect to those of Ar) of the plasma electrons and of the resonant and/or metastable Ar atoms, respectively. In addition, the electron driven ionization and dissociation of C_2H_2 slightly exceed other loss mechanisms of C_2H_2, like Penning ionization and charge transfer ($C_2H_2+Ar^+\rightarrow {C_2H_2}^+ + Ar$). In this regard, the electron-impact ionization and dissociation of C_2H_2 are worth a special comment. Dissociation dominates over ionization but, in addition, the kinetic model indicates that, as the Ar concentration in the plasma grows, the nonequilibrium electron-impact dissociation (and ionization) rates of C_2H_2 remain lower (by roughly one order of magnitude) (see Fig. 4) than their corresponding equilibrium (Maxwellian) rates. The latter behavior is a consequence of the nonequilibrium state of the plasma. This is clearly seen when one calculates the dissociation rate coefficients by using a Maxwellian EEDF and the non-Maxwellian EEDF directly obtained from the solution of the Boltzmann equation taking into account the different kinetic processes considered in our model. The latter calculations are shown in Fig. 4 for each of the average electron energies provided by our model (see Table VI) for the different Ar contents considered.

After the above discussion, we understand that the important Ar-dependent increment in the concentration of C_2 (see Fig. 3) is mainly due to two mechanisms. As the amount of Ar in the plasma increases, the dissociation of C_2H_2 due to collisions with Ar atoms becomes more efficient and, second, much less C_2 is lost through collisions with H_2 since Ar substitutes H_2. Moreover, Eq. (2) indicates that the concentration of C_2* is mainly controlled by electronic excitation from the ground electronic state of C_2 and that it follows the trend of the C_2 concentration as Ar increases. We have schematically represented in Fig. 5 the different reaction paths underlying the values of the concentrations of C_2 and C_2* obtained in the present work.

We would like to end up by pointing out the fact that the analysis of the nonequilibrium plasma chemistry of rf (13.56 MHz) C_2H_2 (1%)/H_2/Ar plasmas suggests that the species C_2 and C_2*, and C_2H rather than C_2H_2 and CH_3 seem to be specially connected with the possible surface growth mechanisms underlying the synthesis of nanodiamond thin films observed within high pressure (50–100 Torr) MW (Refs. 2–10) and medium pressure (0.2–0.8 Torr) rf hydrocarbon/Ar-rich plasmas.[1] In addition, whereas the surface loss (or reaction) probability for CH_3 radicals on the surface of amorphous carbon films is quite low (less than 10^{-2}),[11] that of C_2H is high and reaches values of up to approximately 0.90.[11] The latter could additionally support the possible dominant role of C_2, C_2*, and C_2H species if the nanodiamond phase started in a preliminary phase of amorphous carbon. However, the surface loss probabilities of C_2 or C_2* are not available for any type of growing carbon surface. In addition, no measurements of C_2*, C_2, and C_2H have been performed either in the bulk of rf

(13.56 MHz) $CH_4/H_2/Ar$ and/or C_2H_2 (1%)/H_2/Ar plasmas or in the interface of the plasma and the growing nanodiamond thin films. Therefore, we think that further experimental research is needed in order to experimentally elucidate the role of C_2^*, C_2, and C_2H during the growth mechanisms of nanodiamond thin films in medium pressure rf (13.56 MHz) hydrocarbon/Ar-rich plasmas.

IV. CONCLUSIONS

We have investigated some aspects of the nonequilibrium plasma chemistry of medium pressure (0.75 Torr) rf (13.56 MHz)-produced C_2H_2 (1%)/H_2/Ar-rich plasmas of interest for the synthesis of nanodiamond thin films. Special attention has been paid to the reaction paths underlying the concentration of the dimers C_2 and C_2^*. We found that the important Ar-dependent increase of the C_2 and C_2^* concentrations is the consequence of the combination of an efficient dissociation of C_2H_2 in collisions with Ar atoms, and of the less C_2 losses in collisions with H_2. In addition, we obtained that while the concentration of the species C_2H is also sensitive to the Ar content in the plasma, those of CH_3 and C_2H_2 remain practically constant as it is observed experimentally[12] but contrary to previous simulation results by other authors.[13] Therefore, we think that the influence of the species C_2, C_2^*, and C_2H on the growth mechanisms of the nanodiamond phase is more determinant than the one of the species C_2H_2 and CH_3.

ACKNOWLEDGMENTS

This work was partially funded by CICYT (Spain) under a Ramón y Cajal project and under Project No. TIC2002-03235. One of the authors (F.J.G.V.) acknowledges a Ramón y Cajal contract from the Spanish Ministry of Science and Technology (MCYT). One of the authors (J.M.A.) acknowledges partial support from CICYT (Spain) under Project No. MAT 2002-04085-C02-02.

[1] G. Amaratunga, A. Putnis, K. Clay, and W. Milne, Appl. Phys. Lett. **55**, 634 (1989).
[2] D. M. Gruen, S. Liu, A. R. Krauss, and X. Pan, J. Appl. Phys. **75**, 1758 (1994).
[3] D. M. Gruen, S. Liu, A. R. Krauss, J. Luo, and X. Pan, Appl. Phys. Lett. **64**, 1502 (1994).
[4] D. M. Gruen, C. D. Zuiker, A. R. Krauss, and X. Pan, J. Vac. Sci. Technol. A **13**, 1628 (1995).
[5] D. Zhou, T. G. McCauley, L. C. Qin, A. R. Krauss, and D. M. Gruen, J. Appl. Phys. **83**, 540 (1998).
[6] A. N. Goyette, J. E. Lawler, L. W. Anderson, D. M. Gruen, T. G. McCauley, D. Zhou, and A. R. Krauss, J. Phys. D **31**, 1975 (1998).
[7] D. Zhou, D. M. Gruen, L. C. Qin, T. G. McCauley, and A. R. Krauss, J. Appl. Phys. **84**, 1981 (1998).
[8] T. G. McCauley, D. M. Gruen, and A. R. Krauss, Appl. Phys. Lett. **73**, 1646 (1998).
[9] P. C. Redfern, D. A. Horner, A. A. Curtis, and D. M. Gruen, J. Phys. Chem. **100**, 11654 (1996).
[10] A. N. Goyette, J. E. Lawler, L. W. Anderson, D. M. Gruen, T. G. McCauley, D. Zhou, and A. R. Krauss, Plasma Sources Sci. Technol. **7**, 149 (1998).
[11] A. von Keudell, C. Hopf, T. Schwarz-Selinger, and W. Jacob, Nucl. Fusion **39**, 1451 (1999).
[12] V. Schulz-von der Gathen, J. Röpcke, T. Gans, M. Käning, C. Lukas, and H. F. Döbele, Plasma Sources Sci. Technol. **10**, 530 (2001).
[13] C. Riccardi, R. Barni, M. Fontanesi, and P. Tosi, Chem. Phys. Lett. **329**, 66 (2000).
[14] F. J. Gordillo-Vázquez and J. M. Albella, Plasma Sources Sci. Technol. **11**, 498 (2002).
[15] J. N. Brooks, Z. Wang, D. N. Ruzic, and D. A. Alman, Argonne National Laboratory (Fusion Power Plant) Report No. 297 (1999).
[16] U. Fantz, S. Meir, and M. Berger, in *Proceedings of the Sixteenth European Conference on Atomic and Molecular Physics of Ionized Gases* (ESCAMPIG, Grenoble, France, 2002), Vol. 2, p. 123.
[17] G. Theodorakopoulos and I. D. Petsalakis, J. Chem. Phys. **101**, 194 (1994).
[18] M. T. Jones, T. D. Dreiling, D. W. Setser, and R. N. MacDonald, J. Phys. Chem. **89**, 4501 (1985).
[19] M. Tsuji, H. Kouno, K. Matsumura, T. Funatsu, and Y. Nishimura, J. Chem. Phys. **98**, 2011 (1993).
[20] A. J. M. Buuron, Ph.D. thesis, Eindhoven University of Technology (1993).
[21] H. Tahara, K. Minami, A. Murai, T. Yasui, and T. Yoshikawa, Jpn. J. Appl. Phys., Part 1 **34**, 1972 (1995).
[22] L. E. Kline, W. D. Partlow, and W. E. Bies, J. Appl. Phys. **65**, 70 (1989).
[23] A. J. Dean, R. K. Hanson, and C. T. Bowman, J. Phys. Chem. **95**, 3180 (1991).
[24] R. A. Brownsword, A. Canosa, B. R. Rowe, I. R. Sims, I. W. M. Smith, D. W. A. Stewart, A. C. Symonds, and D. Travers, J. Chem. Phys. **106**, 7662 (1997).
[25] A. Bogaerts and R. Gijbels, Phys. Rev. A **52**, 3743 (1995).
[26] W. L. Morgan, J. P. Boeuf, and L. C. Pitchford, *BOLSIG, a Two-Term Boltzmann Solver*, Kinema Software, 1997 (http://www.kinema.com).
[27] M. Heintze and M. Magureanu, J. Appl. Phys. **92**, 2276 (2002).
[28] H. Reisler, M. S. Mangir, and C. Wittig, J. Chem. Phys. **73**, 2280 (1980).
[29] G. Dinescu, A. de Graaf, E. Aldea, and M. C. M. van de Sanden, Plasma Sources Sci. Technol. **10**, 513 (2001).
[30] A. M. Derkatch, A. Al-Khalili, L. Vikor, A. Neau, W. Shi, H. Donared, M. af Ugglas, and M. Larsson, J. Phys. B **32**, 3391 (1999).